CELL ENGINEERING

Synthetic biology-based cellular biomedical tattoo for detection of hypercalcemia associated with cancer

Aizhan Tastanova,[1] Marc Folcher,[1] Marius Müller,[1] Gieri Camenisch,[1] Aaron Ponti,[1] Thomas Horn,[1] Maria S. Tikhomirova,[1] Martin Fussenegger[1,2]*

Diagnosis marks the beginning of any successful therapy. Because many medical conditions progress asymptomatically over extended periods of time, their timely diagnosis remains difficult, and this adversely affects patient prognosis. Focusing on hypercalcemia associated with cancer, we aimed to develop a synthetic biology-inspired biomedical tattoo using engineered cells that would (i) monitor long-term blood calcium concentration, (ii) detect onset of mild hypercalcemia, and (iii) respond via subcutaneous accumulation of the black pigment melanin to form a visible tattoo. For this purpose, we designed cells containing an ectopically expressed calcium-sensing receptor rewired to a synthetic signaling cascade that activates expression of transgenic tyrosinase, which produces melanin in response to persistently increased blood Ca^{2+}. We confirmed that the melanin-generated color change produced by this biomedical tattoo could be detected with the naked eye and optically quantified. The system was validated in wild-type mice bearing subcutaneously implanted encapsulated engineered cells. All animals inoculated with hypercalcemic breast and colon adenocarcinoma cells developed tattoos, whereas no tattoos were seen in animals inoculated with normocalcemic tumor cells. All tumor-bearing animals remained asymptomatic throughout the 38-day experimental period. Although hypercalcemia is also associated with other pathologies, our findings demonstrate that it is possible to detect hypercalcemia associated with cancer in murine models using this cell-based diagnostic strategy.

INTRODUCTION

Classically, medical treatment begins with diagnosis after the development of subjective symptoms, but this may be too late for the most effective therapy. There is increasing interest in proactive measures to prevent disease, such as raising awareness, encouraging regular medical checkups, screening and monitoring individuals based on family history, risk, or environmental factors, and changing lifestyle (*1*). Personalized, next-generation medicine requires smart diagnostic devices suitable for long-term monitoring of disease-related metabolites and biomarkers to detect the onset or recurrence of pathological conditions at the earliest possible stage and thereby optimize prognosis and treatment success (*2*).

Among potential targets for such devices, cancer is considered a global health priority, with more than 14 million new cases per year, and accounting for about 15% of all deaths (*3*). It is well established that detection of asymptomatic cancer can markedly improve the prognosis (*4*). Many cancers such as breast cancer (*5*), colon cancer, prostate cancer (*6*), lung cancer (*7*), and gastrointestinal (*8*) and hematological malignancies (*9*) are associated with hypercalcemia. Therefore, we hypothesized that monitoring blood calcium concentration could be a suitable strategy to detect these types of cancer at an asymptomatic stage.

Calcium is required by all living cells to maintain normal structure and function (*10*). Its role as a second messenger in signal transduction, managing physiological functions associated with cell proliferation and apoptosis as well as differentiation, cell adhesion, and motility, has been extensively studied (*11*), but its role as a first messenger in the development of cancer has only recently been uncovered (*12*). In humans, calcium is stored in bone as mineralized hydroxyapatite and is present in blood, either as free Ca^{2+} or bound to various carriers such as albumin (*13*). Calcium homeostasis is precisely regulated and restored within minutes after fluctuations by several hormonal systems (*14*). For example, a decrease in blood calcium concentration stimulates parathyroid glands to release parathyroid hormone (PTH), which promotes calcium reabsorption and mobilization from bone. On the other hand, increasing blood Ca^{2+} concentrations activate the calcium-sensing receptor (CaSR), which acutely inhibits the secretion of PTH (*15*). Cancer is among the causes of hypercalcemia (*16*), and humoral hypercalcemia of malignancy is associated with a variety of cancers, including breast (*5*, *16*), colon (*16*), prostate (*7*), lung (*17*), and kidney cancers (*18*). It arises because the primary tumor, its metastases, or immune cells targeting the tumor secrete humoral factors (*16*) that act on bone, kidney, and intestine, thereby disrupting calcium homeostasis and resulting in increased blood-calcium concentration (*19*).

CaSR is a natural hypercalcemia sensor that is sufficiently sensitive to detect mild to moderate hypercalcemia (5.6 to 10 mg Ca^{2+}/dl blood), which often remains unnoticed when a patient is asymptomatic (*13*, *16*) or shows only nonspecific symptoms such as anorexia, anxiety, and weakness (*18*, *20*). Therefore, we considered that CaSR might be suitable for detection of cancer at an early (asymptomatic) stage. Here, we engineered cells to ectopically express CaSR rewired to a synthetic signaling cascade, leading to expression of tyrosinase, which synthesizes the black pigment melanin. We anticipated that the resulting accumulation of melanin by the subcutaneously implanted engineered cells would produce a visible tattoo, thus enabling detection of hypercalcemia associated with asymptomatic cancer. Here, we describe the design and construction of the engineered cells and validate the biomedical tattoo system in wild-type mice bearing subcutaneously implanted encapsulated engineered cells and inoculated with carcinoma cells.

RESULTS

Design and optimization of the synthetic hypercalcemia sensor

The engineered cell–based biomedical tattoo system consists of two main components rewired via synthetic signaling cascades: a hypercalcemia

[1]Department of Biosystems Science and Engineering, ETH Zurich, Mattenstrasse 26, CH-4058 Basel, Switzerland. [2]Faculty of Science, University of Basel, Mattenstrasse 26, CH-4058 Basel, Switzerland.
*Corresponding author. Email: fussenegger@bsse.ethz.ch

biosensor monitoring blood-calcium concentrations and a chimeric hypercalcemia-sensitive biosensor-dependent promoter driving expression of a pigment-producing enzyme that generates a visible skin tattoo (Fig. 1A). The human CaSR, a class C group G protein–coupled receptor (GPCR) managing calcium homeostasis in humans (*21*), serves as the hypercalcemia biosensor (Fig. 1A). Hypercalcemia-mediated activation of CaSR triggers the cell's endogenous calcium-calmodulin-calcineurin-NFAT (nuclear factor of activated T cells) and Raf–$ERK_{1/2}$ (extracellular signal–regulated kinase 1 and 2)–SRE (serum response element) signaling cascades, which induce a synthetic calcium-sensitive promoter (P_{Ca}) driving expression of copper-containing human tyrosinase, the rate-limiting enzyme in the synthesis of the black pigment melanin (Fig. 1A) (*22*). Thus, persistent hypercalcemia is recorded as an accumulation of melanin in subcutaneously implanted engineered cells and visualized as a black skin tattoo.

To test the sensitivity of CaSR to hypercalcemia, we cotransfected human embryonic kidney (HEK) 293 cells with the constitutive CaSR expression vector pAT12 (P_{hCMV}-CaSR-pA) as well as pAT16 (P_{Ca4}-SEAP-pA) encoding the human model glycoprotein SEAP (human placental secreted alkaline phosphatase) under control of a synthetic CaSR-dependent Ca^{2+}-sensitive promoter (P_{Ca4}) containing three SRE and six NFAT operator modules 5′ of a minimal version of the human cytomegalovirus immediate early promoter ($P_{hCMVmin}$) (table S1). Exposing the cultures to increasing Ca^{2+} concentrations showed that these engineered human cells expressed more SEAP under mild hypercalcemia (>1.5 mM Ca^{2+}) compared to control populations that were only transfected with the reporter construct pAT16 (P_{Ca4}-SEAP-pA) (Fig. 1B).

To improve the sensitivity and dynamics of the synthetic hypercalcemia sensor, we constructed an optimized synthetic Ca^{2+}-sensitive promoter (P_{Ca6}) by linking 3 SRE and 15 NFAT operator modules 5′ of a minimal version of the alpha-myosin heavy chain promoter ($P_{\alpha MHCmin}$) (pAT50, P_{Ca6}-SEAP-pA). HEK-293 cells cotransfected with pAT12 and pAT50 showed substantially improved Ca^{2+} responsiveness compared to the original pAT12/pAT16 vector combination (Fig. 1C). Ca^{2+}-responsive SEAP expression seemed to be specific for HEK-293 cells because other cell lines such as Chinese hamster ovary (CHO) K1 cells, cultured human keratinocyte cells (HaCaT), and NIH/3T3 were insensitive to changes in Ca^{2+} concentration (Fig. 1D).

Evaluation of the melanin-producing tattoo component

To find a suitable parental cell background for efficient expression of tyrosinase and optimal production of melanin, we transfected the constitutive mammalian tyrosinase expression vector pAT10 (P_{hCMV}-Tyr-pA) into a variety of cell lines (HEK-293, CHO-K1, NIH/3T3, and HaCaT). We profiled the tyrosinase activity after cultivation for 72 hours and compared it to native tyrosinase-expressing Melan-A cells used as positive control. Among the cell lines, the tyrosinase activity in HEK-293 substantially exceeded those in all other cells, including that achieved in the melanin-producing melanocyte cell line Melan-A (Fig. 1E). HEK-293 was therefore selected for subsequent use.

Design and characterization of the stably transgenic HEK_{Tattoo} cell line

Because the engineered cell–based biomedical tattoo is required to profile and record persistent hypercalcemia over long periods of time, we designed a stably transgenic HEK_{Tattoo} cell line containing the human hypercalcemia sensor CaSR (pAT12, P_{hCMV}-CaSR-pA) and the human melanin-producing tyrosinase driven by a CaSR-dependent Ca^{2+}-sensitive promoter (pAT53, P_{Ca6}-Tyr-pA). Among 57 different stable tattoo clones, the HEK_{Tattoo} cell line showed excellent Ca^{2+}-responsive tyrosinase expression with submillimolar sensitivity (Fig. 2A), which resulted in substantially increased production of melanin in the target range of ≥1.6 mM Ca^{2+} corresponding to mild hypercalcemia (Fig. 2B).

To examine the melanin-production dynamics, we seeded HEK_{Tattoo} cells into individual wells of a 96-well plate containing increasing Ca^{2+} concentrations and recorded melanin production by time-lapse microscopy. Pigment production by HEK_{Tattoo} was compared with that of the positive control, HEK_{Tyr} cells transfected with a constitutive tyrosinase expression vector pAT10 (P_{hCMV}-Tyr-pA) (movies S1 to S5). HEK_{Tattoo} cultured under mild and moderate hypercalcemia (1.6 and 1.8 mM Ca^{2+}, respectively; movies S4 and S5) showed melanin production comparable to that of the positive control (movie S1), whereas no pigment production was observed in HEK_{Tattoo} exposed to low (0.5 mM) or normal (1.3 mM) Ca^{2+} concentrations (movies S2 and S3). Quantitative analysis of melanin production dynamics by HEK_{Tattoo} exposed to mild (1.6 mM Ca^{2+}) and moderate (1.8 mM Ca^{2+}) hypercalcemia confirmed that only persistent hypercalcemia of at least 12 hours (moderate hypercalcemia) and 24 hours (mild hypercalcemia) triggered visible melanin production (Fig. 2C). Because the interplay between calcitonin and the PTH typically restores blood Ca^{2+} homeostasis within minutes (*14*, *23*), the biomedical tattoo is expected to be insensitive to natural Ca^{2+} fluctuations and should only detect persistent hypercalcemia (movies S4 and S5 and Fig. 2C).

Melanin is insoluble and has a half-life of several weeks in the melanocytes of human skin (*24*). To validate whether a biomedical tattoo would remain visible for extended periods of time, we stored hypercalcemia-induced melanin-containing HEK_{Tattoo} pellets for up to 6 months at room temperature. Because the melanin content was almost unchanged over the entire storage period, HEK_{Tattoo}-based melanin production is expected to provide reliable detection of hypercalcemia (Fig. 2D).

To use HEK_{Tattoo} in an in vivo experimental cancer setting with wild-type mice, we microencapsulated the cells in clinically licensed alginate–PLL [poly-(L-lysine)]–alginate beads (*25*). Before implanting the microencapsulated HEK_{Tattoo} cells, we conducted control experiments to confirm that the encapsulated cells still responded efficiently to persistent mild hypercalcemia with visible melanin production and that there was no interference with hypercalcemia detection, recording, or pigmentation due to either transient exposure to Ca^{2+} during alginate polymerization or leaching of Ca^{2+} from the alginate polymer (Fig. 2, E and F). The results indicated that the encapsulated cells retained the desired characteristics. To test the biomedical tattoo in a thick-skin model that is comparable to human skin, we subcutaneously injected microencapsulated HEK_{Tattoo} cells cultivated in normo- and hypercalcemic conditions into porcine skin ex vivo, recorded the resulting visible tattoo (Fig. 2G), and quantified pixel intensities from the corresponding grayscale photographs (Fig. 2H). The visible dark spot produced by hypercalcemic HEK_{Tattoo} implants confirmed that the biomedical tattoo remained visible when injected under thick skin (Fig. 2, G and H).

HEK_{Tattoo}-based detection of cancer-induced hypercalcemia in nude mice

To test whether hypercalcemia-triggered melanin production by HEK_{Tattoo} was sufficient to detect asymptomatic tumor development

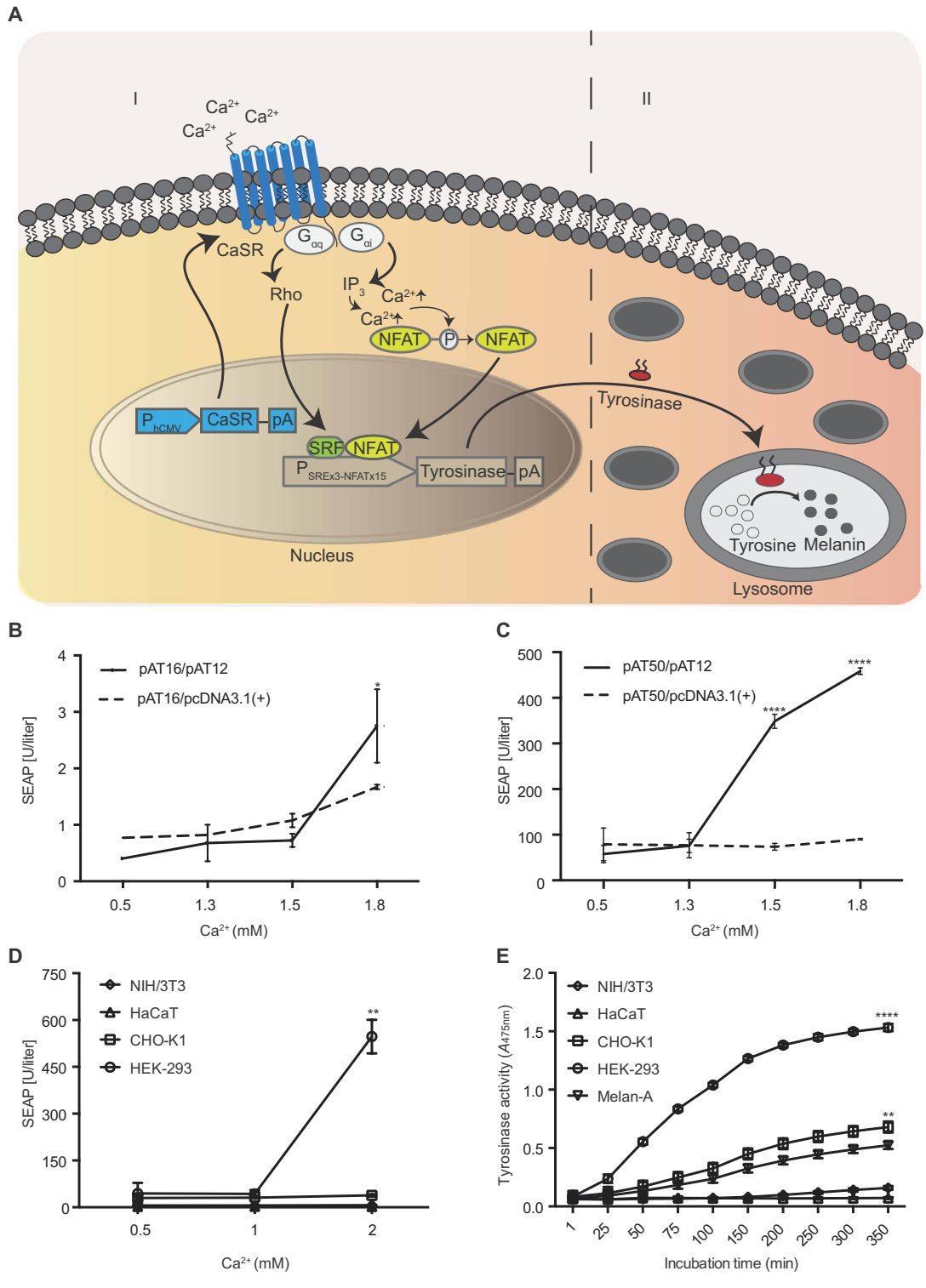

Fig. 1. Design and optimization of the cell-based biomedical tattoo system. (**A**) Molecular mechanism of pigment production by HEK_{Tattoo} cells upon induction by hypercalcemia. The sensing component of the biomedical tattoo system (I) is a calcium-sensing receptor (CaSR), a member of C group G protein–coupled receptors. The visualization component (II) consists of the enzyme tyrosinase, which is usually located in a specialized pigment-producing organelle (the melanosome) in melanocytes, where it catalyzes oxidation of phenols such as tyrosine to form melanin. In nonmelanogenic cells such as human embryonic kidney–293 (HEK-293) cells, tyrosinase is localized in lysosomes, which are closely related to melanosomes and undergo a similar maturation process. IP_3, inositol 1,4,5-trisphosphate; NFAT, nuclear factor of activated T cells; SRF, serum response factor. (**B**) Secreted alkaline phosphatase (SEAP) expression in response to calcium stimulation in HEK-293 cells transiently transfected with a constitutive CaSR construct (pAT12, P_{hCMV}-CaSR-pA) and either an inducible SEAP reporter construct (pAT16, P_{Ca4}-SEAP-pA) or a mock construct [pcDNA3.1(+)]. Increase in SEAP expression compared between 0.5 and 1.8 mM Ca^{2+} concentration, $P = 0.026$, determined using independent t test where $^{*}P < 0.05$. (**C**) Optimization of the reporter construct. NIH/3T3, HaCat, CHO-K1 (Chinese hamster ovary–K1), or HEK-293 cells (7×10^4) were transiently transfected with 500 ng of a constitutive CaSR construct (pAT12, P_{hCMV}-CaSR-pA) and 500 ng of either an optimized inducible SEAP reporter construct (pAT50, P_{Ca6}-SEAP-pA) or a mock construct [pcDNA3.1(+)] and induced with increasing Ca^{2+} concentrations. Increase in SEAP expression compared between 0.5 and 1.5 mM and 1.8 mM Ca^{2+} concentrations, $P < 0.0001$ at both concentrations determined using independent t test where $^{****}P < 0.0001$. (**D**) Cell line screening for SEAP expression. NIH/3T3, HaCat, CHO-K1, or HEK-293 cells (7×10^4) were transiently transfected with 500 ng of a constitutive CaSR construct (pAT12, P_{hCMV}-CaSR-pA) and 500 ng of either an inducible SEAP reporter construct (pAT50, P_{Ca6}-SEAP-pA) or a mock construct [pcDNA3.1(+)] and induced with increasing Ca^{2+} concentrations. Increase in SEAP expression observed in HEK-293 cells between 0.5 and 2 mM Ca^{2+} concentrations, $P = 0.0029$ determined using independent t test ($^{**}P < 0.01$). (**E**) Cell line screening for tyrosinase expression. NIH/3T3, HaCat, CHO-K1, or HEK-293 cells (7×10^4) were transiently transfected with 1 μg of a constitutive tyrosinase construct (pAT10, P_{hCMV}-Tyr-pA). Melan-A cells were used as a positive control. Increased tyrosinase activity compared between Melan-A and CHO-K1 and HEK-293 expressing constitutive tyrosinase, $P = 0.0019$ and $P = 0.0001$, respectively, determined using one-way analysis of variance (ANOVA) with Dunnett's multiple comparison test ($^{**}P < 0.01$ and $^{****}P < 0.0001$). Corresponding reporter concentrations were profiled 72 hours after induction with Ca^{2+}. A_{475nm}, absorbance at 475 nm. All experimental data are presented as means ± SD, $n \geq 3$ independent experiments.

via a visible black skin tattoo, we subcutaneously injected nonencapsulated HEK_{Tattoo} cells into the flank of nude mice with asymptomatic hypercalcemic mammary and colon adenocarcinoma (produced by inoculation of 410.4 or Colon-26 cells) or a normocalcemic adenocarcinoma (produced by inoculation of 168 cell line; negative control) (Fig. 3A). Healthy nude mice injected with nonencapsulated HEK-293 cells engineered for constitutive tyrosinase expression (pAT10, P_{hCMV}-Tyr-pA) were used as a positive control (Fig. 3B). Animals with normocalcemic tumors did not develop any skin tattoos, indicating that our system is specific for hypercalcemia-associated cancer types (Fig. 3, C and D). The hypercalcemia-triggered tyrosinase expression in HEK_{Tattoo} resulted in the accumulation of sufficient melanin to produce a visible diagnostic black spot on the skin of animals bearing hypercalcemic cancers (Fig. 3D), and cancer-associated

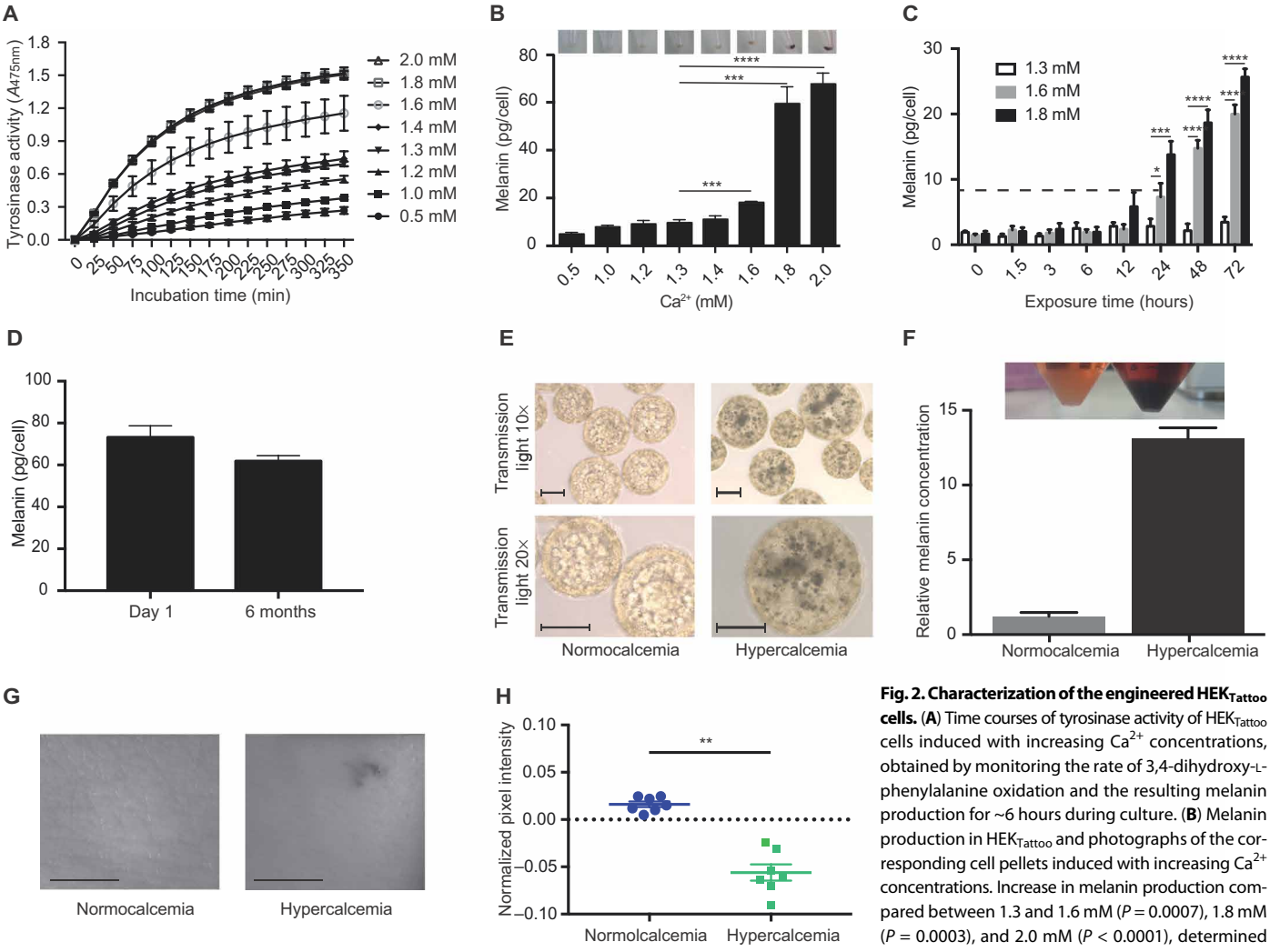

Fig. 2. Characterization of the engineered HEK_{Tattoo} cells. (**A**) Time courses of tyrosinase activity of HEK_{Tattoo} cells induced with increasing Ca^{2+} concentrations, obtained by monitoring the rate of 3,4-dihydroxy-L-phenylalanine oxidation and the resulting melanin production for ~6 hours during culture. (**B**) Melanin production in HEK_{Tattoo} and photographs of the corresponding cell pellets induced with increasing Ca^{2+} concentrations. Increase in melanin production compared between 1.3 and 1.6 mM ($P = 0.0007$), 1.8 mM ($P = 0.0003$), and 2.0 mM ($P < 0.0001$), determined using independent *t* tests. All analyses were performed after 72 hours incubation with Ca^{2+}. Data are shown as means ± SD, $n \geq 3$ independent experiments. (**C**) Melanin production kinetics of HEK_{Tattoo} exposed to normocalcemia (1.3 mM), mild hypercalcemia (1.6 mM), and moderate hypercalcemia (1.8 mM) for different periods of time. Increase in melanin production by HEK_{Tattoo} exposed to Ca^{2+} concentrations of 1.6 and 1.8 compared to 1.3 for different time durations—24 hours: 1.3 mM versus 1.6 and 1.8 mM, $P = 0.0412$ and $P = 0.0006$, respectively; 48 hours: 1.3 mM versus 1.6 and 1.8 mM, $P = 0.0001$ and $P = 0.0001$, respectively; and 72 hours: 1.3 mM versus 1.6 and 1.8 mM, $P = 0.0001$ and $P = 0.0001$, respectively. Statistical significance of differences determined using one-way ANOVA with Dunnett's multiple comparison test. Data are shown as means ± SD, $n \geq 3$ independent experiments. (**D**) Stability of melanin in HEK_{Tattoo} pellets stored for up to 6 months at room temperature. (**E**) In vitro functionality assessment of encapsulated HEK_{Tattoo} cells in response to transient Ca^{2+} exposure. Microscopy images of pelleted microencapsulated HEK_{tattoo} cells incubated under normocalcemic and hypercalcemic conditions. Scale bars, 100 μm. (**F**) Relative melanin concentrations in lysed microencapsulated HEK_{tattoo} and photographs of the corrresponding microencapsulated cell pellets incubated under normocalcemic and hypercalcemic conditions. HEK_{Tattoo} cells were incubated in calcium-free media for 24 hours after encapsulation to allow Ca^{2+} associated with the encapsulation process to diffuse out of the capsules. Images were taken and melanin analysis was performed after incubation at normo- and hypercalcemic concentrations for 96 hours. (**G**) Grayscale microscopy images of porcine skin implanted with Ca^{+}-induced (hypercalcemia) and noninduced (normocalcemia) microencapsulated HEK_{Tattoo} cells. (**H**) Normalized pixel intensities proportional to melanin concentration in ex vivo porcine skin implanted with HEK_{Tattoo} cells treated with hypercalcemic and normocalcemic conditions. HEK_{Tattoo} cells were preincubated in medium containing either 1.3 or 1.8 mM Ca^{2+} before implantation. Images were normalized to have the same mean pixel intensity of the reference standard (black sheet). Scale bars, 500 μm. Data are presented as means ± SEM, and statistical significance of differences between hypercalcemic and normocalcemic groups was calculated using unpaired *t* test ($n = 7$ injection sites) where $^{*}P < 0.05$, $^{**}P < 0.01$, $^{***}P < 0.001$, and $^{****}P < 0.0001$.

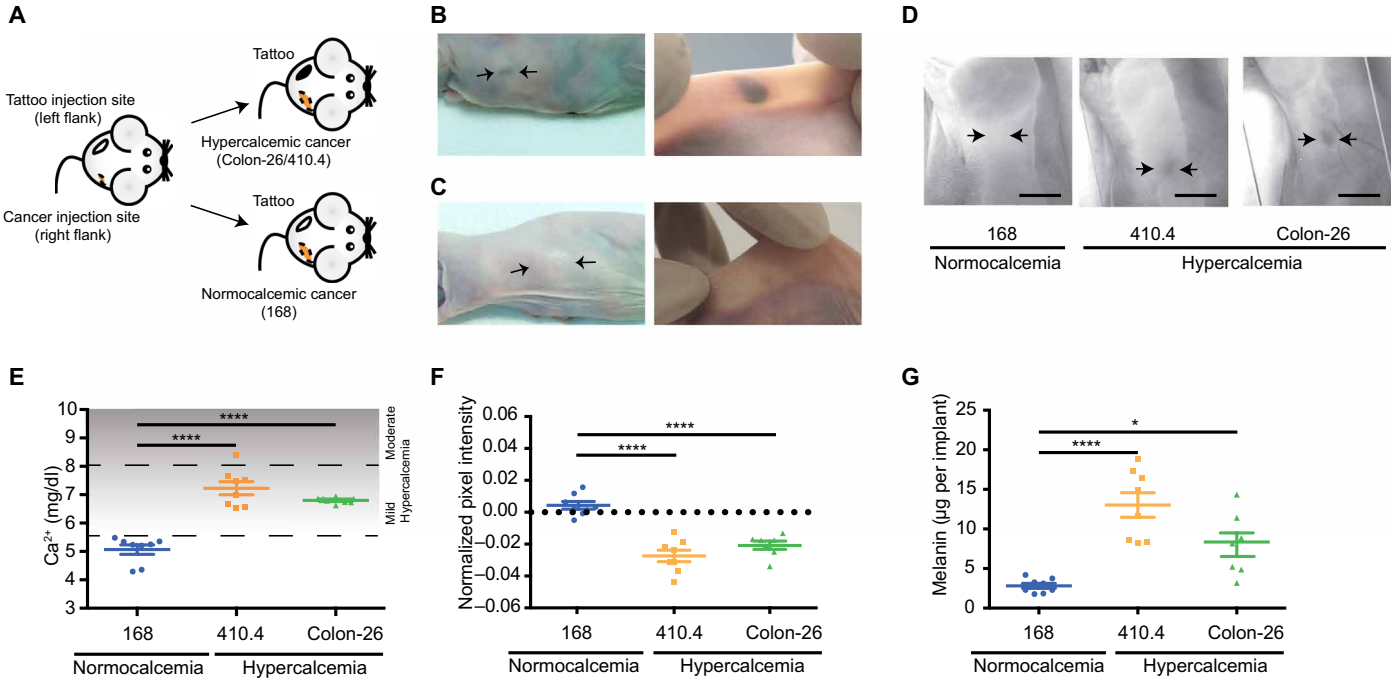

Fig. 3. Application of the biomedical tattoo system in nude mice. (**A**) Schematic representation of the engineered nonencapsulated HEK_{Tattoo} cells implanted into nude mice inoculated with hypercalcemic (HEK-293 with constitutive tyrosine expression, 410.4, and Colon-26 cancer cell lines) and normocalcemic cells (168 cancer cell line). (**B**) Photograph of a mouse from the positive control group implanted with HEK-293 cells constitutively expressing the tyrosinase construct. (**C**) Photograph of a negative control mouse inoculated with normocalcemic cancer (168 cell line) and implanted with HEK_{Tattoo} cells. (**D**) Grayscale microscopy images of the HEK_{Tattoo} implantation site in mice inoculated with 168, 410.4, and Colon-26 cell lines. Scale bars, 8.6 mM. (**E**) Ca^{2+} blood concentrations of mice in the hypercalcemic and normocalcemic groups. 168 versus 410.4 ($P = 0.0001$) and Colon-26 ($P = 0.0001$). Horizontal dashed lines represent hypercalcemia conditions (mild, 5.6 to 8 mg/dl; moderate, 8.1 to 10 mg/dl; severe, >10 mg/dl). (**F**) Normalized pixel intensities extracted from the skin at the implantation site of individual mice from hypercalcemic and normocalcemic groups. 168 versus 410.4 ($P = 0.0001$) and Colon-26 ($P = 0.0001$). Images were normalized to have the same mean pixel intensity of the reference standard (black sheet). (**G**) Melanin extracted from the implantation site of individual mice from hypercalcemic and normocalcemic groups after 24 days. 168 versus 410.4 ($P = 0.0118$) and Colon-26 ($P = 0.0001$). Data are represented as means ± SEM, and statistical significance of differences between hypercalcemic and normocalcemic groups was calculated using one-way ANOVA with Dunnett's multiple comparison test ($n \geq 7$ mice) where $^*P < 0.05$ and $^{****}P < 0.0001$.

hypercalcemia was successfully recorded for over 3 weeks (Fig. 3E). The intensity of the skin tattoo was comparable to the treatment group injected with positive control cells constitutively expressing tyrosinase (Fig. 3B). In addition, profiling of blood Ca^{2+} over the entire 24-day study duration confirmed that skin-tattoo development was associated with the onset of mild hypercalcemia produced by hypercalcemic tumors (Fig. 3E). To profile pigment production by the subcutaneous implants, we quantified pixel intensities in micrographs of the implant sites of all treatment groups. Mice from hypercalcemic groups showed substantially lower normalized pixel intensities (Fig. 3F) due to melanin at the implant site (Fig. 3G) compared to those in normocalcemic animals (Fig. 3, F and G).

Validation of the biomedical tattoo in wild-type mice

Next, we implanted microencapsulated HEK_{Tattoo} subcutaneously into the flank of wild-type mice with asymptomatic hypercalcemic carcinomas (produced by inoculation of 410.4 or Colon-26 cells) or normocalcemic adenocarcinoma (produced by inoculation of 168 cell line; negative control) (Fig. 4A). Healthy mice injected with HEK-293 cells engineered for constitutive tyrosinase expression (pAT10, P_{hCMV}-Tyr-pA) served as positive controls (Fig. 4B). Animals with normocalcemic tumors (negative control) did not produce any skin tattoo, as expected (Fig. 4, C and D). The biomedical tattoo successfully recorded the persistent cancer-associated hypercalcemia in the groups inoculated with 410.4 or Colon-26 cells throughout the experimental period of 38 days (Fig. 4, D and E). Tattoos were quantified by shaving the implantation site and then taking a micrograph of the pinched skin transilluminated with red light. Comparison of the experimental groups showed that a black skin tattoo (Fig. 4D) similar to the tattoo in positive control animals implanted with cells constitutively expressing tyrosinase (Fig. 4B) was visible only in animals with hypercalcemic cancers (Fig. 4D). Profiling of blood Ca^{2+} over the 38-day experimental period confirmed that tattoo formation was associated with the onset of mild hypercalcemia in the groups inoculated with 410.4 and Colon-26 cells (Fig. 4E). All tumor-bearing animals remained asymptomatic throughout the 38-day period. We also quantified pigment production by the subcutaneous implants in all treatment groups. Mice from hypercalcemic groups showed decreased normalized pixel intensities ($P < 0.01$; Fig. 4F) due to increased melanin at the implantation site (Fig. 4G), compared to normocalcemic animals (Fig. 4, F and G). These results support the view that the cell-based biomedical tattoo could detect, record, and visualize the onset of mild hypercalcemia associated with cancer development during the asymptomatic stage.

DISCUSSION

Tattoos have an interesting medical history. For example, it has been suggested that the tattoos overlapping osteoarthritic joints of the

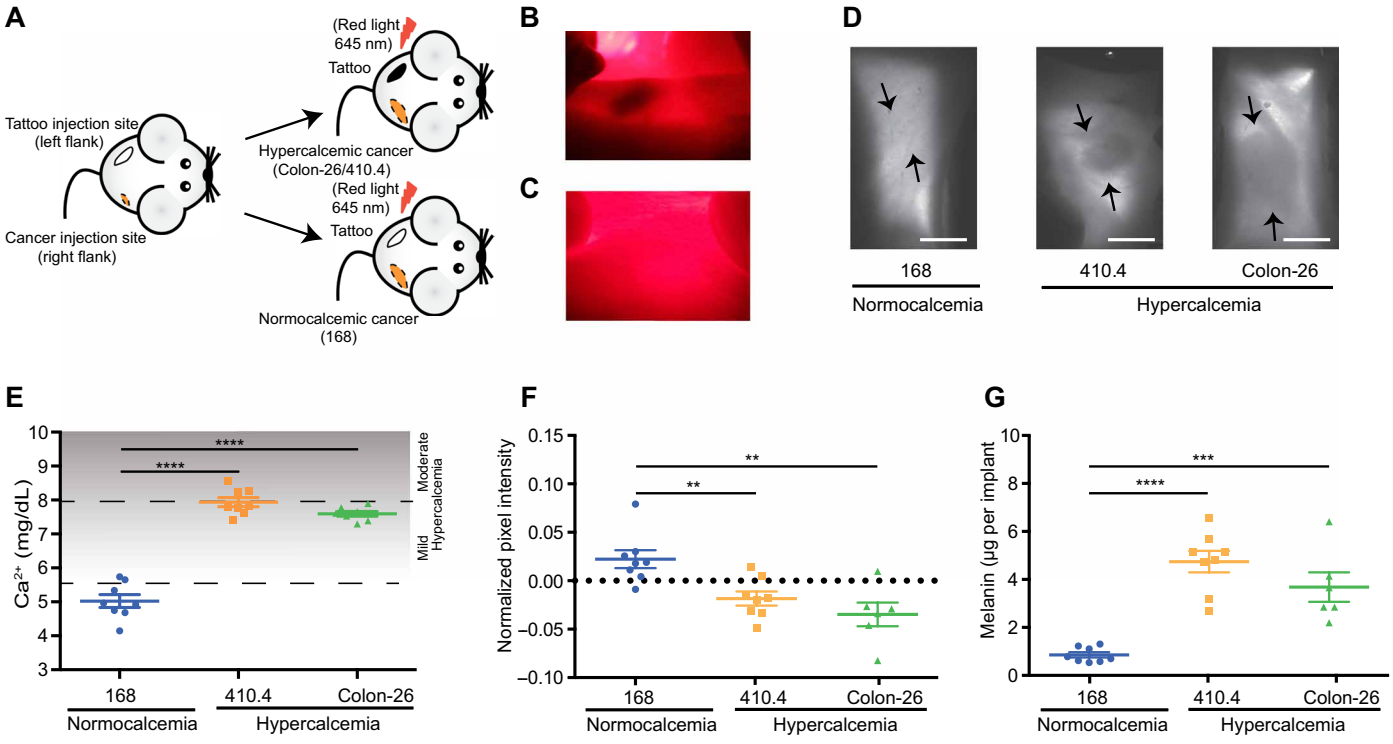

Fig. 4. Application of the biomedical tattoo system in wild-type mice using microencapsulated HEK_{Tattoo} cells. (**A**) Schematic representation of the microencapsulated engineered HEK_{Tattoo} cells implanted into wild-type mice inoculated with hypercalcemic and normocalcemic cancer cells. (**B**) Photograph of a mouse from the positive control group implanted with microencapsulated HEK-293 cells constitutively expressing the tyrosinase construct. (**C**) Photograph of a negative control mouse inoculated with normocalcemic cancer (168 cell line) and implanted with microencapsulated HEK_{Tattoo} cells, illuminated by red light. (**D**) Grayscale microscopy images of the pinched skin transilluminated with red light at the microencapsulated HEK_{Tattoo} implantation site of mice inoculated with 168, 410.4, and Colon-26 cell lines. Scale bars, 8.6 mm. (**E**) Ca^{2+} blood concentrations of mice in the hypercalcemic and normocalcemic groups. 168 versus 410.4 ($P = 0.0001$) and Colon-26 ($P = 0.0001$). Horizontal dashed lines represent hypercalcemia conditions (mild, 5.6 to 8 mg/dl; moderate, 8.1 to 10 mg/dl; severe, >10 mg/dl). The termination point was a tumor size of 10 mm. The last points were collected over 18 days at the terminal tumor size. (**F**) Normalized pixel intensities extracted from the skin images of the implantation site of hypercalcemic and normocalcemic groups after 38 days. 168 versus 410.4 ($P = 0.001$) and Colon-26 ($P = 0.0085$). Images were taken using transillumination at a wavelength of 617 to 645 nm and normalized to have the mean pixel intensity of the reference standard (gray-level reference standard). (**G**) In vivo melanin production by microencapsulated HEK_{Tattoo} cells extracted from the implantation site of mice in the hypercalcemic and normocalcemic groups after 38 days. 168 versus 410.4 ($P = 0.0003$) and Colon-26 ($P = 0.0001$). Data are represented as means ± SEM, and statistical significance of difference between hypercalcemic and normocalcemic groups was calculated using one-way ANOVA with Dunnett's multiple comparison test ($n \geq 6$ mice) where $^{**}P < 0.01$, $^{***}P < 0.001$, and $^{****}P < 0.0001$.

5000-year-old body of iceman Ötzi found in the Tyrolian alps originated from acupuncture-like stimulatory treatment (*26*). In the mid-1850s, medical tattoos were used for the treatment of congenital vascular nevi (*27*). Today, tattooing is considered more effective than intramuscular injection for delivery of certain drugs, as well as DNA and peptide vaccines (*28*), and functionalized subcutaneous nanoparticle tattoos have been successfully applied to optically quantify compounds such as nitric oxide and glucose in the bloodstream using skin-based electronics (*29*–*31*). Work is also proceeding on other applications, such as skin-interfacing wearable electronic devices for the detection of movement disorders (Parkinson's disease) (*32*), heart, brain, and skeletal muscle dysfunctions (based on epidermal electrophysiology) (*33*), infections (based on increased body temperature) (*32*), and glucose, lactate, and electrolyte concentrations in perspiration (*34*).

Melanin is a natural tanning pigment produced from the ubiquitous nonessential amino acid tyrosine by specialized epidermal melanocytes in response to sunlight exposure and serves to protect the skin from ultraviolet radiation–induced damage (*35*). Because of their color, melanin-based biomedical tattoos can easily be qualitatively assessed with the naked eye or quantified using wearable electronics (*36*). Thus, we decided to adopt a melanin-based system in the present work to detect hypercalcemia that is associated with the asymptomatic development of many types of cancer (*5*). We expected that such a system would have practical benefits, because diagnosis of asymptomatic cancer, although difficult, could increase treatment options and improve survival rates (*37*), particularly for individuals with known risk factors (*38*–*40*) and patients who have undergone primary tumor treatment and require continuous monitoring to diagnose cancer recurrence (*41*, *42*) or development of metastases (*43*, *44*).

To engineer the required implantable cells for detection of mild hypercalcemia as a biomedical tattoo, we used synthetic biology principles (*45*–*47*) to rewire the calcium sensor CaSR to expression of melanin. The challenges included (i) achieving suitable sensitivity to detect the onset of persistent mild hypercalcemia, (ii) providing high specificity for hypercalcemia, and (iii) ensuring low basal expression of melanin. The engineered HEK_{Tattoo} cells met these criteria; in particular, we observed no false-positive tattoo formation in negative-control treatment groups throughout the 38-day experimental period.

The systemic and intracellular calcium signaling is tightly controlled and essential for normal physiological functioning of cellular processes. Tight control within the cell, where Ca^{2+} serves as a second messenger, is maintained through various calcium pumps, channels, and calcium-binding proteins (*48*). The dysregulation in intracellular Ca^{2+} homeostasis may result in cancer initiation, progression, and angiogenesis. Therefore, many cancer therapies target intracellular calcium by affecting Ca^{2+} channels and pumps (*49*). Because the biomedical tattoo specifically senses only the systemic Ca^{2+} concentrations that are 20,000-fold higher than those promoting intracellular Ca^{2+} signaling, the sensitivity and performance of the biomedical tattoo are not expected to be compromised by Ca^{2+}-specific metabolic activities.

As a natural skin pigment, melanin is particularly well suited for a biomedical tattoo. We confirmed that the tattoo was insensitive to short-term Ca^{2+} fluctuations as well as leaky accumulation and was stable for at least 6 months. In addition, melanin absorbs light over a wide spectrum. Possible interference with darker skin tones may be alleviated by depigmentation of the biomedical tattoo area using a number of available medical procedures such as laser and lightening agents (*50*). Although the melanin-based biomedical tattoo has been developed and validated for the detection and diagnosis of hypercalcemia associated with cancer, it may in principle be linked to other biosensors and serve as a diagnostic device for the detection of a wider range of medical conditions.

The aim of the biomedical tattoo is to detect asymptomatic mild hypercalcemia associated with cancer. Hypercalcemia develops from mild via moderate to high hypercalcemia. During this trajectory, the biomedical tattoo detects persistent mild hypercalcemia, which may indicate an emerging health issue that requires further attention. In mouse models inoculated with colon and breast cancer cell lines known to be associated with hypercalcemia, the biomedical tattoo reliably detected the development of cancer that was still at an asymptomatic stage. Hypercalcemia is not exclusively linked to cancer development but is also associated with other pathologies, including hyperparathyroidism (*5*), granulomatous disease (*5*), cognitive dysfunction (*51*), renal failure (*52*), and cardiac arrhythmia (*53*). Although these medical conditions are usually symptomatic and typically only emerge during hypercalcemia, which may discriminate them from asymptomatic cancer, the biomedical tattoo could also produce false-positive events and detect medical conditions unrelated to cancer (*20*, *54*). Therefore, the use of a biomedical tattoo for the diagnosis of hypercalcemia associated with cancer would be best indicated for individuals with known risk factors for colon cancer [loss of CaSR expression (*55*), ectopic PTH secretion (*56*, *57*), and ulcerative colitis (*58*, *59*)] and breast cancer [human epidermal growth factor receptor-2–positive status (*38*), parathyroid hormone-related protein overexpression (*40*), and ectopic expression of PTH (*60*)] and for patients who have undergone primary tumor treatment and require continuous monitoring to diagnose cancer recurrence (*41*, *42*), as well as the development of metastases (*43*, *44*).

Like any cell-based therapy, the biomedical tattoo requires a minimally invasive procedure that places microencapsulated engineered cells under the skin. However, considering the severity of the disease and the focus on patients with known risk factors and primary therapy, acceptance of the potential risks related to surgical intervention (*61*) and leakage of the encapsulation device (*62*) seems justifiable. Alginate-based encapsulation of cells, as used in our proof-of-concept study, has been clinically licensed (*25*), and other laminated membrane–based implant devices are currently being tested in human clinical trials (*63*). Once the biomedical tattoo has diagnosed hypercalcemia, it has served its purpose and can either be removed or replaced. Only heterologous engineered cells will need encapsulation to protect the biomedical tattoo from the host immune system. Because the entire tattoo, including CaSR, tyrosinase, and melanin as well as the signaling cascade and the promoter, consists of nonmodified endogenous components, their introduction into autologous cells would create a biomedical tattoo device that could be directly injected subcutaneously. After an autologous biomedical tattoo has served its purpose, it may simply be left in place, and a new biomedical tattoo could be injected at another site to monitor cancer recurrence or development of metastases.

Early enough diagnosis during the asymptomatic phase of a developing medical condition represents the key to prevention and successful therapy. In conclusion, the present work provides an important proof of concept of this new diagnostic strategy, demonstrating the feasibility of using engineered cell–based biomedical tattoos for surveillance and potential detection of asymptomatic cancers based on mild hypercalcemia.

MATERIALS AND METHODS

Study design

The goal of this study was to design a cell-based biomedical tattoo that, upon subcutaneous implantation, constantly monitored blood calcium and produced a visible melanin-based black mark on the skin in response to persistent mild hypercalcemia. The biomedical tattoo is expected to provide visual diagnosis of a hypercalcemia-associated emerging medical condition that requires further medical attention. As a proof-of-concept hypercalcemia-associated medical condition, we chose asymptomatic colon and breast cancer to validate the biomedical tattoo in mouse models in vivo. The tattoo was designed by rewiring Ca^{2+}-mediated activation of the ectopically expressed CaSR to the chimeric promoter P_{Ca6} via a synthetic signaling cascade, which triggers Ca^{2+}-responsive expression of tyrosinase, eventually producing the black skin pigment melanin. After assembling, optimizing, and validating the individual components in HEK-293 cells, we generated a stably transgenic HEK_{Tattoo} cell line that produced the expected hypercalcemia-associated melanin-based black skin tattoo in porcine skin mimicking human skin. Next, we validated the biomedical tattoo for diagnosis of asymptomatic breast and colon cancer in nude and wild-type mice using subcutaneous implantation of native or microencapsulated HEK_{Tattoo} cells, respectively. For precise quantifications of skin tattoos, we developed a tailored MATLAB code (see MATLAB code in the Supplementary Materials) for comparative analysis of pixel intensities across different skin samples. Animals were randomly assigned to experimental groups. Investigators were not blinded to tumor inoculation groups. Animals in all treatment groups were implanted with the same number of HEK_{Tattoo} cells. In vitro experiments were performed in triplicate each containing four samples. In vivo studies included up to eight mice per treatment group as specified in the figure legends. Blood samples were collected and frozen after each experiment and simultaneously analyzed after termination of the study.

Plasmid design

Comprehensive design and construction details for all expression vectors are provided in table S1. All relevant genetic components were confirmed by sequencing (Microsynth). The key genetic components of the

biomedical tattoo include (i) the constitutive human tyrosinase expression vector pAT10 (P_{hCMV}-Tyr-pA), (ii) pAT12 (P_{hCMV}-CaSR-pA) encoding constitutive expression of the human CaSR, (iii) the Ca^{2+}-inducible SEAP expression vector pAT50 (P_{Ca6}-SEAP-pA; P_{Ca6}, SRE_3-$NFAT_{15}$-$P_{\alpha MHCmin}$), and (iv) the Ca^{2+}-inducible human tyrosinase expression vector pAT53 (P_{Ca6}-Tyr-pA).

Cell culture and transfection

HEK cells [HEK-293; CRL-11268, American Type Culture Collection (ATCC)], human keratinocytes (HaCaT; Cell Lines Service), mouse fibroblasts (NIH/3T3; CRL-1658, ATCC), and the murine mammary adenocarcinoma cell lines 410.4 and 168 (catalog no. 412005, Barbara Ann Karmanos Cancer Institute) were cultivated in calcium-free Dulbecco's modified Eagle's medium (E15-078, PAA Laboratories) supplemented with 10% fetal calf serum (FCS; catalog no. F7524 and lot no. 022M3395, Sigma-Aldrich), 6 mM L-glutamine (200 mM; catalog no. 25030-024, Invitrogen), and 1% (v/v) penicillin/streptomycin solution (catalog no. L0022-100, Biowest). The colon carcinoma cell line Colon-26 (National Cancer Institute, The Division of Cancer Treatment and Diagnosis Tumor Repository) was cultivated in RPMI 1640 medium (catalog no. E15-885, GE Healthcare) supplemented with 10% FCS and 1% (v/v) penicillin/streptomycin solution. CHO cells (CHO-K1; CCL-61, ATCC) were cultivated in ChoMaster HTS medium (catalog no. CHTS-0.5, Cell Culture Technologies GmbH) supplemented with 5% FCS and 1% (v/v) penicillin/streptomycin solution. These cell lines were cultivated at 37°C in a humidified atmosphere containing 5% CO_2. Human melanoma cells (WM-1650) and mouse melanocytes (Melan-A) (all from Wellcome Trust Functional Genomics Cell Bank) were cultivated in RPMI 1640 medium supplemented with 10% FCS, 1% (v/v) penicillin/streptomycin solution, and 200 nM phorbol 12-myristate 13-acetate (catalog no. P8139, Sigma-Aldrich). All melanocytic cell lines were cultivated at 37°C in a humidified atmosphere containing 10% CO_2. All cell lines were transfected using an optimized polyethyleneimine (PEI)–based protocol. Briefly, 1.5×10^5 cells/ml were seeded per well of a multiwell plate or per cell-culture dish (500 μl per well of a 24-well plate, 1 ml per well of a 12-well plate, 2 ml of a 6-well plate, 10 ml for a 10-cm cell-culture dish) and cultivated for 16 hours before they were transfected by dropwise addition of a transfection solution containing 1 μg of total plasmid DNA, 100 μl of the corresponding FCS-free culture medium, and 3 μl of PEI [PEI "Max"; molecular weight, 40,000; 1 mg/ml in double-distilled water (ddH_2O); catalog no. 24765-2, Polysciences). After 6 hours, the cell culture medium was replaced, and the transfected cells were cultivated for another 12 hours before they were used for a dedicated experiment. The cell number and cell viability were profiled using a CASY Cell Counter and Analyser System Model TT (Roche Diagnostics GmbH).

Design of the transgenic HEK_{Tattoo} cell line

HEK_{Tattoo} was designed by a sequential two-step procedure that initially generated stably CaSR-transgenic $HEK_{CaSR\text{-}1}$ cell clones, which were subsequently engineered for CaSR-dependent Ca^{2+}-inducible human tyrosinase expression. Therefore, 3.5×10^5 HEK-293 cells were seeded per well of a six-well plate, cultivated for 24 hours, and cotransfected with a transfection solution containing 10.5 μl of PEI (1 mg/ml in ddH_2O) as well as 3.5 μg of the constitutive CaSR expression vector pAT12 (P_{hCMV}-CaSR-pA) and 0.35 μg of pcDNA6/V5-HisB (P_{SV40}-bla-pA) conferring blasticidin resistance. After 6 hours, the culture medium was replaced, and the cells were cultivated for 24 hours. A stable mixed population was selected for 7 days in blasticidin-containing medium [blasticidin (1.5 μl/ml) and stock solution (10 mg/ml); catalog no. ant-bl-1 and lot. no. BLL-35-13B, InvivoGen]. After limiting dilution and clonal expansion for 14 days in blasticidin-containing cell culture medium, individual clonal populations were transfected with pAT50 (P_{Ca6}-SEAP-pA) and exposed to increasing Ca^{2+} concentrations for 48 hours, and then the SEAP expression in the culture supernatant were profiled. $HEK_{CaSR\text{-}1}$ showed the best Ca^{2+}-inducible SEAP expression dynamics among 36 tested cell clones and was therefore used as the parental cell line for the production of HEK_{Tattoo}. Then, 3.5×10^5 $HEK_{CaSR\text{-}1}$ cells were seeded per well of a six-well plate, cultivated for 24 hours, and cotransfected with a transfection solution containing 10.5 μl of PEI (1 mg/ml in ddH_2O) as well as 3.5 μg of the Ca^{2+}-inducible human tyrosinase expression vector pAT53 (P_{Ca6}-Tyr-pA) and 0.35 μg of pZeoSV2(+) (P_{hCMV}-zeo-pA) conferring Zeocin resistance. After 6 hours, the culture medium was exchanged, and the cells were cultivated for 24 hours; a stable mixed population was selected for 7 days in blasticidin- and Zeocin-containing medium [Zeocin (1 μl/ml) and stock solution (1 mg/ml); catalog no. ant-zn-1 and lot. no. ZEL-31-313, InvivoGen]. After limiting dilution and clonal expansion for 14 days in blasticidin- and Zeocin-containing cell culture medium, individual clonal populations were exposed to 1.8 mM Ca^{2+} and profiled for tyrosinase activity and production of melanin. HEK_{Tattoo} showed the best Ca^{2+}-inducible melanin expression dynamics among 56 tested cell clones and was therefore used to generate the cancer-specific biomedical tattoo.

Analytical assays

SEAP expression

SEAP production was quantified in cell-culture supernatants by monitoring *p*-nitrophenyl phosphate (pNPP)–based light absorbance. Briefly, 200 μl of cell culture supernatant was heat-inactivated for 30 min at 65°C. Subsequently, 80 μl of the supernatant was transferred to a well of a 96-well plate containing 100 μl of 2× SEAP assay buffer [20 mM homoarginine, 1 mM $MgCl_2$, and 21% (v/v) diethanolamine (pH 9.8); all from Sigma-Aldrich). After the addition of 20 μl of 120 mM pNPP (disodium salt, hexahydrate, Acros Organics BVBA) and dilution in 1× SEAP assay buffer, the time-dependent increase in light absorbance was determined at 405 nm and 37°C for 30 min using a 2104 EnVision multilabel plate reader (PerkinElmer).

Melanin production

A total of 1×10^5 cells cultivated in monolayer cultures, 200 μg of explanted tissue, or 200 μg of explanted alginate-encapsulated cells whose alginate capsules had been degraded by alginate lyase (catalog no. A1603, Sigma-Aldrich) were trypsinized (catalog no. 59430C, Sigma-Aldrich), resuspended in 1 N NaOH (catalog no. S8526, Sigma-Aldrich) and 10% dimethyl sulfoxide (cat. no. 276855, Sigma Aldrich), and incubated for 2 hours at 80°C. Samples were centrifuged for 10 min at 12,000*g* and 22°C, and the supernatants were transferred to the wells of a 96-well plate for measurement of the absorbance at 470 nm using a 2104 EnVision multilabel plate reader. Melanin concentration was calculated on the basis of a standard curve prepared with synthetic melanin (catalog no. M8631-100MG, Sigma-Aldrich) covering a pigment concentration range of 0 to 20 μg/ml.

Tyrosinase activity

Monolayer cultures were trypsinized, or the alginate capsules of microencapsulated cells were degraded by alginate lyase, and the cell suspension was pelleted. The cell pellet was resuspended in 100 μl of phosphate-buffered saline (PBS) (pH 6.8) (catalog no. D8537, Sigma-Aldrich) containing 1% Triton-100 (catalog no. 3051.4, Carl Roth)

and 1× protease inhibitor cocktail (25× stock solution in 2 ml of ddH_2O; catalog no. 11873580001, Roche Diagnostics) and then sonicated for 30 s using a Bioruptor (Diagenode). The lysate was centrifuged for 10 min at 12,000 rpm at 4°C to remove cell debris. Ninety microliters of the lysate was transferred to each well of a 96-well plate, and 10 μl of freshly prepared L-dopa (1 mg/ml in PBS; 3,4-dihydroxy-L-phenylalanine, catalog no. D9628 and lot. no. SLBF6724V, Sigma-Aldrich) was added immediately before starting the assay. Tyrosinase activity was quantified in terms of L-dopa oxidation by measuring dopachrome production for 4 hours at 475 nm using a 2104 EnVision multilabel plate reader.

Calcium concentration

Ca^{2+} concentrations in culture media and blood samples were quantified using a Calcium Colorimetric Assay Kit (Biovision). Briefly, 10 μl of the sample was diluted in 50 μl of ddH_2O and mixed with 90 μl of the chromogenic reagent before adding 60 μl of the calcium assay buffer. The mixture was incubated for 10 min at 22°C and quantified at 575 nm compared to standardized Ca^{2+} samples, using a 2104 EnVision multilabel plate reader (PerkinElmer).

HEK_{Tattoo} implants

Implants were produced by microencapsulating HEK_{Tattoo} cells in coherent alginate-PLL-alginate beads (400 μm; 200 cells per capsule) using an Inotech Encapsulator Research Unit IE-50R (Buechi Labortechnik AG) set to the following parameters: 0.2-mm nozzle with a vibration frequency of 1025 Hz, 25-ml syringe operated at a flow rate of 410 units, and 1.12 kV for bead dispersion. For ex vivo implantation, 7×10^6 microencapsulated HEK_{Tattoo} cells were treated with normo- and hypercalcemic conditions and injected subcutaneously into fresh porcine skin (Kuhn butcher shop), and the samples were analyzed as described in the "Imaging and image analysis" section.

Animal study

All experiments involving animals were performed in accordance with the Swiss animal welfare act and ordinance provided by the veterinary office of the Canton of Basel-Stadt (approval no. 2629/27063). For tumor inoculation, 150 μl of PBS containing 0.5×10^6 (Balb/c-nude mice) or 2×10^6 (wild-type Balb/c mice) cells of the 410.4 (hypercalcemic), Colon-26 (hypercalcemic), or 168 (normocalcemic; negative control) cell lines was subcutaneously injected into the right flank of wild-type Balb/c (BALB/cJRj, Janvier Labs) or Balb/c-nude (BALB/cAnNRj-Foxn1nu, Janvier Labs) mice, and tumors were allowed to form and grow for 2 weeks (tumor diameter, <10 mm). Then, the animals received implants of nonencapsulated (Balb/c-nude mice, 4×10^6 HEK_{Tattoo} cells, subcutaneous, left shoulder) or microencapsulated (wild-type Balb/c mice, 7×10^6 HEK_{Tattoo} cells, subcutaneous, left flank) HEK_{Tattoo} cells. Upon detection of tumor-associated hypercalcemia, HEK_{Tattoo} cells triggered tyrosinase expression, which resulted in the production of melanin, a black pigment that can be directly seen and measured as a dark spot on the skin (Balb/c-nude mice) or determined by transilluminating the pinched skin with red light (wild-type Balb/c mice). For the monitoring of animals, general well-being of the animals was routinely monitored by animal facility caretakers by means of daily visual inspections. Project-specific monitoring was carried out at least three times per week by a veterinarian, and animals were euthanized if symptoms of pain and/or distress were observed. The following humane endpoints were applied: tumor diameter > 10 mm, ulcerations or bleeding, body condition scoring < 2, abnormal breathing pattern, apathy or immobility, closed eyes or self-mutilation, detachment from the group or disinterest in the environment, unkempt appearance such as tangled fur, and discoloration due to secretions. The absence of all those criteria was defined as an asymptomatic disease state in the tumor-inoculated mice.

Imaging and image analysis

All images of the HEK_{Tattoo} implantation sites (left shoulder/flank) were recorded using a Nikon SMZ25 stereo-zoom microscope (0.5× objective and 0.63 zoom; Nikon Instruments GmbH) equipped with a Hamamatsu ORCA-Flash 4.0 digital camera (Hamamatsu Photonics) set to a binning of 2 and an exposure time of 100 ms. To compare the amount of melanin in the tattoos of different mice, we measured and compared their pixel intensities in the corresponding images. Darker areas in the image correspond to lower pixel intensities (black corresponds to a pixel intensity of 0), and lighter areas correspond to higher pixel intensities [white corresponds to a pixel intensity of 65,535 (16 bit)]. For our analysis, the images are normalized to the 0 to 1 range (where 1 corresponds to the maximum value of the detector). Because the skin within the positive melanin-containing tattoo is darker than the surrounding skin, the pixel intensities within the tattoo are lower.

For Balb/c-nude mice, images of the implant site (left shoulder/flank) were taken with incident white light illumination. A black sheet serving as black-level reference standard was placed adjacent to the implantation site, and the pixel intensities of the implantation site were normalized to the mean intensity of the reference standard. In wild-type Balb/c mice, the implantation site (left shoulder/flank area) was shaved, pinched, and transilluminated with red light using a Lumencor SpectraX light engine [645 nm, 50% red-light intensity set with SPECTRA GUI software (Lumencor)] connected via a liquid light guide to a Nikon C-HGFIB collimator (Nikon Instruments GmbH). To transilluminate the skin, we placed the collimator 5 cm below the pinched implantation site. Photographic step tablets (21 steps; catalog no. 1523422, Kodak) were used as gray-level reference standards to normalize the pixel intensity at the implantation site. Image-based quantification of melanin concentration at the implantation site of Balb/c-nude and wild-type Balb/c mice was performed using custom-programmed MATLAB software (MathWorks; see MATLAB code in the Supplementary Materials). Differences in skin color among animals were compensated by subtracting the median intensity of the skin around each implantation site from the intensity at the implantation site itself. The amount of melanin at the implantation site was quantified in terms of mean pixel intensity.

Statistical analysis

All statistical tests were performed using GraphPad Prism software (GraphPad Software Inc.). Fold changes between $\log_{10}$-transformed SEAP values derived from in vitro experiments were compared using independent *t* test (Fig. 1C). All experimental data are presented as means ± SD, $n = 3$ independent experiments. Melanin concentrations of treated HEK_{Tattoo} were analyzed using one-way analysis of variance (ANOVA) with Dunnett's multiple comparison test (Fig. 2C). Differences in normalized pixel intensities recorded from images of porcine skin injected with induced and uninduced microencapsulated HEK_{Tattoo} were compared using independent *t* test (Fig. 2H). Melanin concentrations, normalized pixel intensities, and Ca^{2+} concentrations in treated animals implanted with hypercalcemic 410.4 or Colon-26 cells were compared to those of the control mice implanted with the normocalcemic 168 cell line using GraphPad Prism software (GraphPad Software Inc.) and one-way ANOVA with Dunnett's multiple comparison test. All treatment groups consisted of at least eight

mice ($n = 8$). Data represent the means ± SEM. Differences were considered significant at values of $^{*}P < 0.05$, $^{**}P < 0.01$, and $^{***}P < 0.001$ (Figs. 3, E to G, and 4, E to G). Individual subject-level data are reported in table S2.

SUPPLEMENTARY MATERIALS

www.sciencetranslationalmedicine.org/cgi/content/full/10/437/eaap8562/DC1
Table S1. Plasmids used and designed in this study.
Table S2. Individual subject-level data.
Movie S1. Melanin production by HEK_{Tyr} cells.
Movie S2. HEK_{Tattoo} cells cultured in hypocalcemic medium.
Movie S3. HEK_{Tattoo} cells cultured in normocalcemic medium.
Movie S4. HEK_{Tattoo} cells cultured in mild hypercalcemic medium.
Movie S5. HEK_{Tattoo} cells cultured in moderate hypercalcemic medium.
MATLAB code
References (*64*–*67*)

REFERENCES AND NOTES

1. Q. Tian, N. D. Price, L. Hood, Systems cancer medicine: Towards realization of predictive, preventive, personalized and participatory (P4) medicine. *J. Intern. Med.* **271**, 111–121 (2012).
2. M. Song, H.-W. Lee, D. Kang, The potential application of personalized preventive research. *Jpn. J. Clin. Oncol.* **44**, 1017–1024 (2014).
3. R. Lozano, M. Naghavi, K. Foreman, S. Lim, K. Shibuya, V. Aboyans, J. Abraham, T. Adair, R. Aggarwal, S. Y. Ahn, M. Alvarado, H. R. Anderson, L. M. Anderson, K. G. Andrews, C. Atkinson, L. M. Baddour, S. Barker-Collo, D. H. Bartels, M. L. Bell, E. J. Benjamin, D. Bennett, K. Bhalla, B. Bikbov, A. Bin Abdulhak, G. Birbeck, F. Blyth, I. Bolliger, S. Boufous, C. Bucello, M. Burch, P. Burney, J. Carapetis, H. Chen, D. Chou, S. S. Chugh, L. E. Coffeng, S. D. Colan, S. Colquhoun, K. E. Colson, J. Condon, M. D. Connor, L. T. Cooper, M. Corriere, M. Cortinovis, K. C. de Vaccaro, W. Couser, B. C. Cowie, M. H. Criqui, M. Cross, K. C. Dabhadkar, N. Dahodwala, D. De Leo, L. Degenhardt, A. Delossantos, J. Denenberg, D. C. Des Jarlais, S. D. Dharmaratne, E. R. Dorsey, T. Driscoll, H. Duber, B. Ebel, P. J. Erwin, P. Espindola, M. Ezzati, V. Feigin, A. D. Flaxman, M. H. Forouzanfar, F. G. Fowkes, R. Franklin, M. Fransen, M. K. Freeman, S. E. Gabriel, E. Gakidou, F. Gaspari, R. F. Gillum, D. Gonzalez-Medina, Y. A. Halasa, D. Haring, J. E. Harrison, R. Havmoeller, R. J. Hay, B. Hoen, P. J. Hotez, D. Hoy, K. H. Jacobsen, S. L. James, R. Jasrasaria, S. Jayaraman, N. Johns, G. Karthikeyan, N. Kassebaum, A. Keren, J. P. Khoo, L. M. Knowlton, O. Kobusingye, A. Koranteng, R. Krishnamurthi, M. Lipnick, S. E. Lipshultz, S. L. Ohno, J. Mabweijano, M. F. MacIntyre, L. Mallinger, L. March, G. B. Marks, R. Marks, A. Matsumori, R. Matzopoulos, B. M. Mayosi, J. H. McAnulty, M. M. McDermott, J. McGrath, G. A. Mensah, T. R. Merriman, C. Michaud, M. Miller, T. R. Miller, C. Mock, A. O. Mocumbi, A. A. Mokdad, A. Moran, K. Mulholland, M. N. Nair, L. Naldi, K. M. Narayan, K. Nasseri, P. Norman, M. O'Donnell, S. B. Omer, K. Ortblad, R. Osborne, D. Ozgediz, B. Pahari, J. D. Pandian, A. P. Rivero, R. P. Padilla, F. Perez-Ruiz, N. Perico, D. Phillips, K. Pierce, C. A. Pope III, E. Porrini, F. Pourmalek, M. Raju, D. Ranganathan, J. T. Rehm, D. B. Rein, G. Remuzzi, F. P. Rivara, T. Roberts, F. R. De Leon, L. C. Rosenfeld, L. Rushton, R. L. Sacco, J. A. Salomon, U. Sampson, E. Sanman, D. C. Schwebel, M. Segui-Gomez, D. S. Shepard, D. Singh, J. Singleton, K. Sliwa, E. Smith, A. Steer, J. A. Taylor, B. Thomas, I. M. Tleyjeh, J. A. Towbin, T. Truelsen, E. A. Undurraga, N. Venketasubramanian, L. Vijayakumar, T. Vos, G. R. Wagner, M. Wang, W. Wang, K. Watt, M. A. Weinstock, R. Weintraub, J. D. Wilkinson, A. D. Woolf, S. Wulf, P. H. Yeh, P. Yip, A. Zabetian, Z. J. Zheng, A. D. Lopez, C. J. Murray, M. A. AlMazroa, Z. A. Memish, Global and regional mortality from 235 causes of death for 20 age groups in 1990 and 2010: A systematic analysis for the Global Burden of Disease Study 2010. *Lancet* **380**, 2095–2128 (2012).
4. World Health Organization, "Early detection of cancer," www.who.int/cancer/detection/en/ [Accessed June 2014].
5. A. F. Stewart, Clinical practice. Hypercalcemia associated with cancer. *N. Engl. J. Med.* **352**, 373–379 (2005).
6. J. Liao, A. Schneider, N. S. Datta, L. K. McCauley, Extracellular calcium as a candidate mediator of prostate cancer skeletal metastasis. *Cancer Res.* **66**, 9065–9073 (2006).
7. G. Amuthan, G. Biswas, H. K. Ananadatheerthavarada, C. Vijayasarathy, H. M. Shephard, N. G. Avadhani, Mitochondrial stress-induced calcium signaling, phenotypic changes and invasive behavior in human lung carcinoma A549 cells. *Oncogene* **21**, 7839–7849 (2002).
8. K. Nakajima, M. Tamai, S. Okaniwa, Y. Nakamura, M. Kobayashi, T. Niwa, N. Horigome, N. Ito, S. Suzuki, S. Nishio, M. Komatsu, Humoral hypercalcemia associated with gastric carcinoma secreting parathyroid hormone: A case report and review of the literature. *Endocr. J.* **60**, 557–562 (2013).
9. J. T. S. Sargent, O. P. Smith, Haematological emergencies managing hypercalcaemia in adults and children with haematological disorders. *Br. J. Haematol.* **149**, 465–477 (2010).
10. H. Rasmussen, The calcium messenger system (1). *N. Engl. J. Med.* **314**, 1094–1101 (1986).
11. E. M. Brown, R. J. MacLeod, Extracellular calcium sensing and extracellular calcium signaling. *Physiol. Rev.* **81**, 239–297 (2001).
12. K. Hizaki, H. Yamamoto, H. Taniguchi, Y. Adachi, M. Nakazawa, T. Tanuma, N. Kato, Y. Sukawa, J. V. Sanchez, H. Suzuki, S. Sasaki, K. Imai, Y. Shinomura, Epigenetic inactivation of calcium-sensing receptor in colorectal carcinogenesis. *Mod. Pathol.* **24**, 876–884 (2011).
13. M. F. Carroll, D. S. Schade, A practical approach to hypercalcemia. *Am. Fam. Physician* **67**, 1959–1966 (2003).
14. J. A. Beto, The role of calcium in human aging. *Clin. Nutr. Res.* **4**, 1–8 (2015).
15. D. Riccardi, G. Valenti, Localization and function of the renal calcium-sensing receptor. *Nat. Rev. Nephrol.* **12**, 414–425 (2016).
16. W. Goldner, Cancer-related hypercalcemia. *J. Oncol. Pract.* **12**, 426–432 (2016).
17. X. Li, Z. Bie, Z. Zhang, Y. Li, X. Hu, W. Liu, S. Zhang, G. Cheng, B. Ai, Clinical analysis of 64 patients with lung-cancer-associated hypercalcemia. *J. Cancer Res. Ther.* **11** (Suppl.), C275–C279 (2015).
18. A. E. Mirrakhimov, Hypercalcemia of malignancy: An update on pathogenesis and management. *N. Am. J. Med. Sci.* **7**, 483–493 (2015).
19. W. J. Burtis, T. L. Wu, K. L. Insogna, A. F. Stewart, Humoral hypercalcemia of malignancy. *Ann. Intern. Med.* **108**, 454–457 (1988).
20. S. Minisola, J. Pepe, S. Piemonte, C. Cipriani, The diagnosis and management of hypercalcaemia. *BMJ* **350**, h2723 (2015).
21. E. M. Brown, G. Gamba, D. Riccardi, M. Lombardi, R. Butters, O. Kifor, A. Sun, M. A. Hediger, J. Lytton, S. C. Hebert, Cloning and characterization of an extracellular Ca^{2+}-sensing receptor from bovine parathyroid. *Nature* **366**, 575–580 (1993).
22. M. Benathan, V. Virador, M. Furumura, N. Kobayashi, R. G. Panizzon, V. J. Hearing, Co-regulation of melanin precursors and tyrosinase in human pigment cells: Roles of cysteine and glutathione. *Cell. Mol. Biol.* **45**, 981–990 (1999).
23. M. Peacock, Calcium metabolism in health and disease. *Clin. J. Am. Soc. Nephrol.* **5** (suppl. 1), S23–S30 (2010).
24. N. Mujahid, Y. Liang, R. Murakami, H. G. Choi, A. S. Dobry, J. Wang, Y. Suita, Q. Y. Weng, J. Allouche, L. V. Kemeny, A. L. Hermann, E. M. Roider, N. S. Gray, D. E. Fisher, A UV-independent topical small-molecule approach for melanin production in human skin. *Cell Rep.* **19**, 2177–2184 (2017).
25. D. Jacobs-Tulleneers-Thevissen, M. Chintinne, Z. Ling, P. Gillard, L. Schoonjans, G. Delvaux, B. L. Strand, F. Gorus, B. Keymeulen, D. Pipeleers; Beta Cell Therapy Consortium EU-FP7, Sustained function of alginate-encapsulated human islet cell implants in the peritoneal cavity of mice leading to a pilot study in a type 1 diabetic patient. *Diabetologia* **56**, 1605–1614 (2013).
26. K. Spindler, [The man in the ice under special consideration of paleo-pathological evidence]. *Verh. Dtsch. Ges. Pathol.* **85**, 229–236 (2001).
27. S. Vassileva, E. Hristakieva, Medical applications of tattooing. *Clin. Dermatol.* **25**, 367–374 (2007).
28. D. Pokorná, I. Poláková, M. Kindlová, M. Dušková, V. Ludviková, P. Gabriel, L. Kutinová, M. Müller, M. Šmahel, Vaccination with human papillomavirus type 16-derived peptides using a tattoo device. *Vaccine* **27**, 3519–3529 (2009).
29. P. W. Barone, M. S. Strano, Single walled carbon nanotubes as reporters for the optical detection of glucose. *J. Diabetes Sci. Technol.* **3**, 242–252 (2009).
30. J.-H. Kim, D. A. Heller, H. Jin, P. W. Barone, C. Song, J. Zhang, L. J. Trudel, G. N. Wogan, S. R. Tannenbaum, M. S. Strano, The rational design of nitric oxide selectivity in single-walled carbon nanotube near-infrared fluorescence sensors for biological detection. *Nat. Chem.* **1**, 473–481 (2009).
31. N. M. Iverson, P. W. Barone, M. Shandell, L. J. Trudel, S. Sen, F. Sen, V. Ivanov, E. Atolia, E. Farias, T. P. McNicholas, N. Reuel, N. M. A. Parry, G. N. Wogan, M. S. Strano, In vivo biosensing via tissue-localizable near-infrared-fluorescent single-walled carbon nanotubes. *Nat. Nanotechnol.* **8**, 873–880 (2013).
32. D. L. Chandler, John Rogers and the ultrathin limits of technology: His flexible, skin-mounted biostamp is changing the game for wearable diagnostic devices. *IEEE Pulse* **7**, 9–12 (2016).
33. D.-H. Kim, N. Lu, R. Ma, Y.-S. Kim, R.-H. Kim, S. Wang, J. Wu, S. M. Won, H. Tao, A. Islam, K. J. Yu, T.-i. Kim, R. Chowdhury, M. Ying, L. Xu, M. Li, H.-J. Chung, H. Keum, M. McCormick, P. Liu, Y.-W. Zhang, F. G. Omenetto, Y. Huang, T. Coleman, J. A. Rogers, Epidermal electronics. *Science* **333**, 838–843 (2011).
34. W. Gao, S. Emaminejad, H. Y. Y. Nyein, S. Challa, K. Chen, A. Peck, H. M. Fahad, H. Ota, H. Shiraki, D. Kiriya, D.-H. Lien, G. A. Brooks, R. W. Davis, A. Javey, Fully integrated wearable sensor arrays for multiplexed in situ perspiration analysis. *Nature* **529**, 509–514 (2016).
35. C. R. Goding, Melanocytes: The new black. *Int. J. Biochem. Cell Biol.* **39**, 275–279 (2007).
36. C. Qin, K. Cheng, K. Chen, X. Hu, Y. Liu, X. Lan, Y. Zhang, H. Liu, Y. Xu, L. Bu, X. Su, X. Zhu, S. Meng, Z. Cheng, Tyrosinase as a multifunctional reporter gene for photoacoustic/MRI/PET triple modality molecular imaging. *Sci. Rep.* **3**, 1490 (2013).
37. D. Jelovac, D. K. Armstrong, Recent progress in the diagnosis and treatment of ovarian cancer. *CA Cancer J. Clin.* **61**, 183–203 (2011).

38. H. Sigvaldason, A. Obayan, K. von Kuster, K. A. Pathak, Hypercalcemia in metastatic breast cancer unrelated to skeletal metastasis. *CMAJ* **188**, E91–E94 (2016).
39. H. Hampel, W. L. Frankel, E. Martin, M. Arnold, K. Khanduja, P. Kuebler, H. Nakagawa, K. Sotamaa, T. W. Prior, J. Westman, J. Panescu, D. Fix, J. Lockman, I. Comeras, A. de la Chapelle, Screening for the Lynch syndrome (hereditary nonpolyposis colorectal cancer). *N. Engl. J. Med.* **352**, 1851–1860 (2005).
40. M. Ghoussaini, O. Fletcher, K. Michailidou, C. Turnbull, M. K. Schmidt, E. Dicks, J. Dennis, Q. Wang, M. K. Humphreys, C. Luccarini, C. Baynes, D. Conroy, M. Maranian, S. Ahmed, K. Driver, N. Johnson, N. Orr, I. dos Santos Silva, Q. Waisfisz, H. Meijers-Heijboer, A. G. Uitterlinden, F. Rivadeneira; Netherlands Collaborative Group on Hereditary Breast and Ovarian Cancer (HEBON), P. Hall, K. Czene, A. Irwanto, J. Liu, H. Nevanlinna, K. Aittomäki, C. Blomqvist, A. Meindl, R. K. Schmutzler, B. Müller-Myhsok, P. Lichtner, J. Chang-Claude, R. Hein, S. Nickels, D. Flesch-Janys, H. Tsimiklis, E. Makalic, D. Schmidt, M. Bui, J. L. Hopper, C. Apicella, D. J. Park, M. Southey, D. J. Hunter, S. J. Chanock, A. Broeks, S. Verhoef, F. B. L. Hogervorst, P. A. Fasching, M. P. Lux, M. W. Beckmann, A. B. Ekici, E. Sawyer, I. Tomlinson, M. Kerin, F. Marme, A. Schneeweiss, C. Sohn, B. Burwinkel, P. Guénel, T. Truong, E. Cordina-Duverger, F. Menegaux, S. E. Bojesen, B. G. Nordestgaard, S. F. Nielsen, H. Flyger, R. L. Milne, M. R. Alonso, A. González-Neira, J. Benítez, H. Anton-Culver, A. Ziogas, L. Bernstein, C. C. Dur, H. Brenner, H. Müller, V. Arndt, C. Stegmaier; Familial Breast Cancer Study (FBCS), C. Justenhoven, H. Brauch, T. Brüning; Gene Environment Interaction of Breast Cancer in Germany (GENICA) Network, S. Wang-Gohrke, U. Eilber, T. Dörk, P. Schürmann, M. Bremer, P. Hillemanns, N. V. Bogdanova, N. N. Antonenkova, Y. I. Rogov, J. H. Karstens, M. Bermisheva, D. Prokofieva, E. Khusnutdinova, A. Lindblom, S. Margolin, A. Mannermaa, V. Kataja, V.-M. Kosma, J. M. Hartikainen, D. Lambrechts, B. T. Yesilyurt, G. Floris, K. Leunen, S. Manoukian, B. Bonanni, S. Fortuzzi, P. Peterlongo, F. J. Couch, X. Wang, K. Stevens, A. Lee, G. G. Giles, L. Baglietto, G. Severi, C. McLean, G. G. Alnæs, V. Kristensen, A.-L. Børrensen-Dale, E. M. John, A. Miron, R. Winqvist, K. Pylkäs, A. Jukkola-Vuorinen, S. Kauppila, I. L. Andrulis, G. Glendon, A. M. Mulligan, P. Devilee, C. J. van Asperen, R. A. E. M. Tollenaar, C. Seynaeve, J. D. Figueroa, M. Garcia-Closas, L. Brinton, J. Lissowska, M. J. Hooning, A. Hollestelle, R. A. Oldenburg, A. M. W. van den Ouweland, A. Cox, M. W. R. Reed, M. Shah, A. Jakubowska, J. Lubinski, K. Jaworska, K. Durda, M. Jones, M. Schoemaker, A. Ashworth, A. Swerdlow, J. Beesley, X. Chen; kConFab Investigators; Australian Ovarian Cancer Study Group, K. R. Muir, A. Lophatananon, S. Rattanamongkongul, A. Chaiwerawattana, D. Kang, K.-Y. Yoo, D.-Y. Noh, C.-Y. Shen, J.-C. Yu, P.-E. Wu, C.-N. Hsiung, A. Perkins, R. Swann, L. Velentzis, D. M. Eccles, W. J. Tapper, S. M. Gerty, N. J. Graham, B. A. J. Ponder, G. Chenevix-Trench, P. D. P. Pharoah, M. Lathrop, A. M. Dunning, N. Rahman, J. Peto, D. F. Easton, Genome-wide association analysis identifies three new breast cancer susceptibility loci. *Nat. Genet.* **44**, 312–318 (2012).
41. J. T. Thompson, E. H. Paschold, E. A. Levine, Paraneoplastic hypercalcemia in a patient with adenosquamous cancer of the colon. *Am. Surg.* **67**, 585–588 (2001).
42. R. J. Galindo, I. Romao, A. Valsamis, S. Weinerman, Y. T. Harris, Hypercalcemia of malignancy and colorectal cancer. *World J. Oncol.* **7**, 5–12 (2016).
43. J. Li, A. C. Karaplis, D. C. Huang, P. M. Siegel, A. Camirand, X. F. Yang, W. J. Muller, R. Kremer, PTHrP drives breast tumor initiation, progression, and metastasis in mice and is a potential therapy target. *J. Clin. Invest.* **121**, 4655–4669 (2011).
44. X. Shen, L. Qian, M. Falzon, PTH-related protein enhances MCF-7 breast cancer cell adhesion, migration, and invasion via an intracrine pathway. *Exp. Cell Res.* **294**, 420–433 (2004).
45. W. C. Ruder, T. Lu, J. J. Collins, Synthetic biology moving into the clinic. *Science* **333**, 1248–1252 (2011).
46. L. Schukur, B. Geering, G. Charpin-El Hamri, M. Fussenegger, Implantable synthetic cytokine converter cells with AND-gate logic treat experimental psoriasis. *Sci. Transl. Med.* **7**, 318ra201 (2015).
47. M. Xie, H. Ye, H. Wang, G. Charpin-El Hamri, C. Lormeau, P. Saxena, J. Stelling, M. Fussenegger, β-cell–mimetic designer cells provide closed-loop glycemic control. *Science* **354**, 1296–1301 (2016).
48. M. J. Berridge, M. D. Bootman, H. L. Roderick, Calcium signalling: Dynamics, homeostasis and remodelling. *Nat. Rev. Mol. Cell Biol.* **4**, 517–529 (2003).
49. X. Ding, Z. He, K. Zhou, J. Cheng, H. Yao, D. Lu, R. Cai, Y. Jin, B. Dong, Y. Xu, Y. Wang, Essential role of TRPC6 channels in G2/M phase transition and development of human glioma. *J. Natl. Cancer Inst.* **102**, 1052–1068 (2010).
50. S. Briganti, E. Camera, M. Picardo, Chemical and instrumental approaches to treat hyperpigmentation. *Pigment Cell Res.* **16**, 101–110 (2003).
51. E. Shane, D. Irani, Hypercalcemia: Pathogenesis clinical manifestations, differential diagnosis, and management, in *Primer on the Metabolic Bone Diseases and Disorders of Mineral Metabolism*, M. J. Favus, Ed. (American Society for Bone and Mineral Research, ed. 6, 2006), pp. 176–180.
52. T. Amin, P. T. Coates, J. Barbara, P. Hakendorf, N. Karim, Prevalence of hypercalcaemia in a renal transplant population: A single centre study. *Int. J. Nephrol.* **2016**, 7126290 (2016).
53. L. C. Wesson, V. Suresh, R. G. Parry, Severe hypercalcaemia mimicking acute myocardial infarction. *Clin. Med.* **9**, 186–187 (2009).
54. R. Carroll, G. Matfin, Endocrine and metabolic emergencies: Hypercalcaemia. *Ther. Adv. Endocrinol. Metab.* **1**, 225–234 (2010).
55. S. Tennakoon, A. Aggarwal, E. Kállay, The calcium-sensing receptor and the hallmarks of cancer. *Biochim. Biophys. Acta* **1863**, 1398–1407 (2016).
56. D. S. Feig, I. S. Gottesman, Familial hyperparathyroidism in association with colonic carcinoma. *Cancer* **60**, 429–432 (1987).
57. R. J. MacLeod, Extracellular calcium-sensing receptor/PTH knockout mice colons have increased Wnt/β-catenin signaling, reduced non-canonical Wnt signaling, and increased susceptibility to azoxymethane-induced aberrant crypt foci. *Lab. Invest.* **93**, 520–527 (2013).
58. N. J. Petrelli, A. A. Valle, T. K. Weber, M. Rodriguez-Bigas, Adenosquamous carcinoma of the colon and rectum. *Dis. Colon Rectum* **39**, 1265–1268 (1996).
59. F. Michelassi, A. G. Montag, G. E. Block, Adenosquamous-cell carcinoma in ulcerative colitis. Report of a case. *Dis. Colon Rectum* **31**, 323–326 (1988).
60. M. Sztern, A. Barkan, E. Rakowsky, R. Shainkin-Kestenbaum, R. Marilus, I. Blum, Hypercalcemia in carcinoma of the breast without evidence of bone destruction: Beneficial effect of hormonal therapy. *Cancer* **48**, 2383–2385 (1981).
61. A. Heile, T. Brinker, Clinical translation of stem cell therapy in traumatic brain injury: The potential of encapsulated mesenchymal cell biodelivery of glucagon-like peptide-1. *Dialogues Clin. Neurosci.* **13**, 279–286 (2011).
62. E. Santos, J. L. Pedraz, R. M. Hernandez, G. Orive, Therapeutic cell encapsulation: Ten steps towards clinical translation. *J. Control. Release* **170**, 1–14 (2013).
63. E. Motté, E. Szepessy, K. Suenens, G. Stangé, M. Bomans, D. Jacobs-Tulleneers-Thevissen, Z. Ling, E. Kroon, D. Pipeleers; Beta Cell Therapy Consortium EU-FP7, Composition and function of macroencapsulated human embryonic stem cell-derived implants: Comparison with clinical human islet cell grafts. *Am. J. Physiol. Endocrinol. Metab.* **307**, E838–E846 (2014).
64. J. C. Braz, O. F. Bueno, Q. Liang, B. J. Wilkins, Y.-S. Dai, S. Parsons, J. Braunwart, B. J. Glascock, R. Klevitsky, T. F. Kimball, T. E. Hewett, J. D. Molkentin, Targeted inhibition of p38 MAPK promotes hypertrophic cardiomyopathy through upregulation of calcineurin-NFAT signaling. *J. Clin. Invest.* **111**, 1475–1486 (2003).
65. S. A. Stanley, J. E. Gagner, S. Damanpour, M. Yoshida, J. S. Dordick, J. M. Friedman, Radio-wave heating of iron oxide nanoparticles can regulate plasma glucose in mice. *Science* **336**, 604–608 (2012).
66. G. Lennon, C. Auffray, M. Polymeropoulos, M. B. Soares, The I.M.A.G.E. Consortium: An integrated molecular analysis of genomes and their expression. *Genomics* **33**, 151–152 (1996).
67. H. Ye, M. Daoud-El Baba, R.-W. Peng, M. Fussenegger, A synthetic optogenetic transcription device enhances blood-glucose homeostasis in mice. *Science* **332**, 1565–1568 (2011).

Acknowledgments: We are grateful to H. Zulewski, P. Saxena, T. Rubic-Schneider, and J. Moggs for advice and critical comments on the manuscript, and we thank D. Zimmer and M.-D. Hussherr for conducting animal experiments. We are grateful to A. Alitalo for helping to design the animal study. We thank H.-M. Kaltenbach for his valuable support with statistical analyses. This work was supported by the National Centre of Competence in Research (NCCR) for Molecular Systems Engineering. **Funding:** This work was supported by a grant of the Swiss NCCR Molecular Systems Engineering to M. Fussenegger. **Author contributions:** A.T., M. Folcher, and M. Fussenegger designed the project and analyzed the results. A.T., M.M., T.H., and A.P. performed the experimental work. A.T., A.P., and M.S.T. designed and wrote the MATLAB code. A.T. and G.C. designed the animal experiments. A.T. and M. Fussenegger wrote the manuscript. **Competing interests:** The authors declare that they have no competing financial interests. **Data and materials availability:** All data necessary for the interpretation of results are included in the paper and the Supplementary Materials. Requests for additional information and materials should be directed to the corresponding author.

Submitted 2 September 2017
Accepted 29 March 2018
Published 18 April 2018
10.1126/scitranslmed.aap8562

Citation: A. Tastanova, M. Folcher, M. Müller, G. Camenisch, A. Ponti, T. Horn, M. S. Tikhomirova, M. Fussenegger, Synthetic biology-based cellular biomedical tattoo for detection of hypercalcemia associated with cancer. *Sci. Transl. Med.* **10**, eaap8562 (2018).

Science Translational Medicine

Synthetic biology-based cellular biomedical tattoo for detection of hypercalcemia associated with cancer

Aizhan Tastanova, Marc Folcher, Marius Müller, Gieri Camenisch, Aaron Ponti, Thomas Horn, Maria S. Tikhomirova and Martin Fussenegger

Sci Transl Med **10**, eaap8562.
DOI: 10.1126/scitranslmed.aap8562

A melanin mark for hypercalcemia

Earlier detection of disease could help improve response to therapy. Blood calcium concentrations are elevated in several types of cancer, in addition to other diseases. Here, Tastanova *et al*. used synthetic biology and cell engineering to develop a sensor that detects hypercalcemia. Their implantable sensor consists of cells that express the calcium-sensing receptor and produce melanin in response to sustained elevated calcium in the blood. Melanin was visible as a dark pigment in the encapsulated cell constructs in vitro and could be detected when implanted in pig skin ex vivo. Melanin production was also observed in engineered cells implanted in mice bearing hypercalcemic breast and colon cancer tumors. This biomedical tattoo strategy could also potentially be used to noninvasively monitor response to treatment.